nature communications

Article

https://doi.org/10.1038/s41467-024-52466-4

Distinct ventral hippocampal inhibitory microcircuits regulating anxiety and fear behaviors

Received: 17 November 2023

Accepted: 6 September 2024

Published online: 19 September 2024

Check for updates

Kaizhen Li[1], Konstantinos Koukoutselos[1], Masanori Sakaguchi[2] & Stéphane Ciocchi[1]

In emotion research, anxiety and fear have always been interconnected, sharing overlapping brain structures and neural circuitry. Recent investigations, however, have unveiled parallel long-range projection pathways originating from the ventral hippocampus, shedding light on their distinct roles in anxiety and fear. Yet, the mechanisms governing the emergence of projection-specific activity patterns to mediate different negative emotions remain elusive. Here, we show a division of labor in local GABAergic inhibitory microcircuits of the ventral hippocampus, orchestrating the activity of subpopulations of pyramidal neurons to shape anxiety and fear behaviors in mice. These findings offer a comprehensive insight into how distinct inhibitory microcircuits are dynamically engaged to encode different emotional states.

Anxiety and fear reflect negative emotional states that trigger different defensive behaviors to promote survival in hazardous environments[1–4]. Anxiety is evoked by potential and anticipated threats, whereas fear is elicited by more concrete and acute threats[2,4]. Multiple brain regions are involved in detecting and evaluating threat stimuli and subsequently triggering the expression of anxiety or fear behaviors. Among these regions the amygdala, ventral hippocampus and medial prefrontal cortex are pivotal in threat evaluation, anxiety processing, and fear encoding[5–7], with their strong interconnections via diverse and parallel long-range projections underscoring the complexity of emotion processing[8–17]. Strikingly, recent research has identified specific long-range projection pathways in the ventral CA1 hippocampus (vCA1) that play distinct roles in anxiety and fear behaviors[18–20]. Specifically, vCA1 projections to the lateral hypothalamus and medial prefrontal cortex are associated with anxiety-related experiences[18,19], whereas vCA1 projections to the amygdala mediate context-dependent fear[13,21,22]. However, the precise mechanisms coordinating these parallel vCA1 projection pathways during anxiety and fear remain unclear. In clinical practice, benzodiazepines, which allosterically modulate γ-aminobutyric acid (GABA) A receptors, are the most commonly prescribed anxiolytic drugs[23]. Yet, it remains to be determined whether distinct vCA1 GABA-releasing interneurons are differentially involved in anxiety and fear.

In this study, we used in vivo calcium imaging and optogenetic manipulation of vCA1 pyramidal neurons and subclasses of interneurons in freely behaving mice to test whether there are selective inhibitory microcircuits for anxiety and fear in the vCA1. Our results suggest that distinct ventral hippocampal inhibitory microcircuits underlie anxiety and fear behaviors.

Results

Distinct subpopulations of vCA1 pyramidal neurons represent anxiety and fear

To explore how the vCA1 region encodes anxiety and fear-related behaviors, we employed the genetically encoded Ca^{2+} indicator GCaMP6f to image Ca^{2+} signals in individual vCA1 pyramidal neurons. This was achieved using a GRIN lens and a head-mounted miniature microscope in freely behaving mice[24,25] (Fig. 1a and Supplementary Fig. 1b). The mice were initially subjected to anxiety-inducing tasks, specifically the elevated plus maze (EPM) and a forced anxiety-shifting task (FAST[26], see "Methods"). The FAST, akin to the EPM, capitalizes on the innate anxiety of open spaces and height, but, contrary to the EPM, forces mice to confront an anxiogenic environment across multiple trials while alternating with a safe and enclosed environment (Fig. 1b). The FAST started with 5 trials to evaluate novelty-related activity followed by 10 trials to assess anxiety-related activity with exposure to a

[1]Laboratory of Systems Neuroscience, Department of Physiology, University of Bern, Bern, Switzerland. [2]International Institute for Integrative Sleep Medicine, University of Tsukuba, Tsukuba, Japan. e-mail: kaizhen.li@unibe.ch; stephane.ciocchi@unibe.ch

https://doi.org/10.1038/s41467-024-52466-4

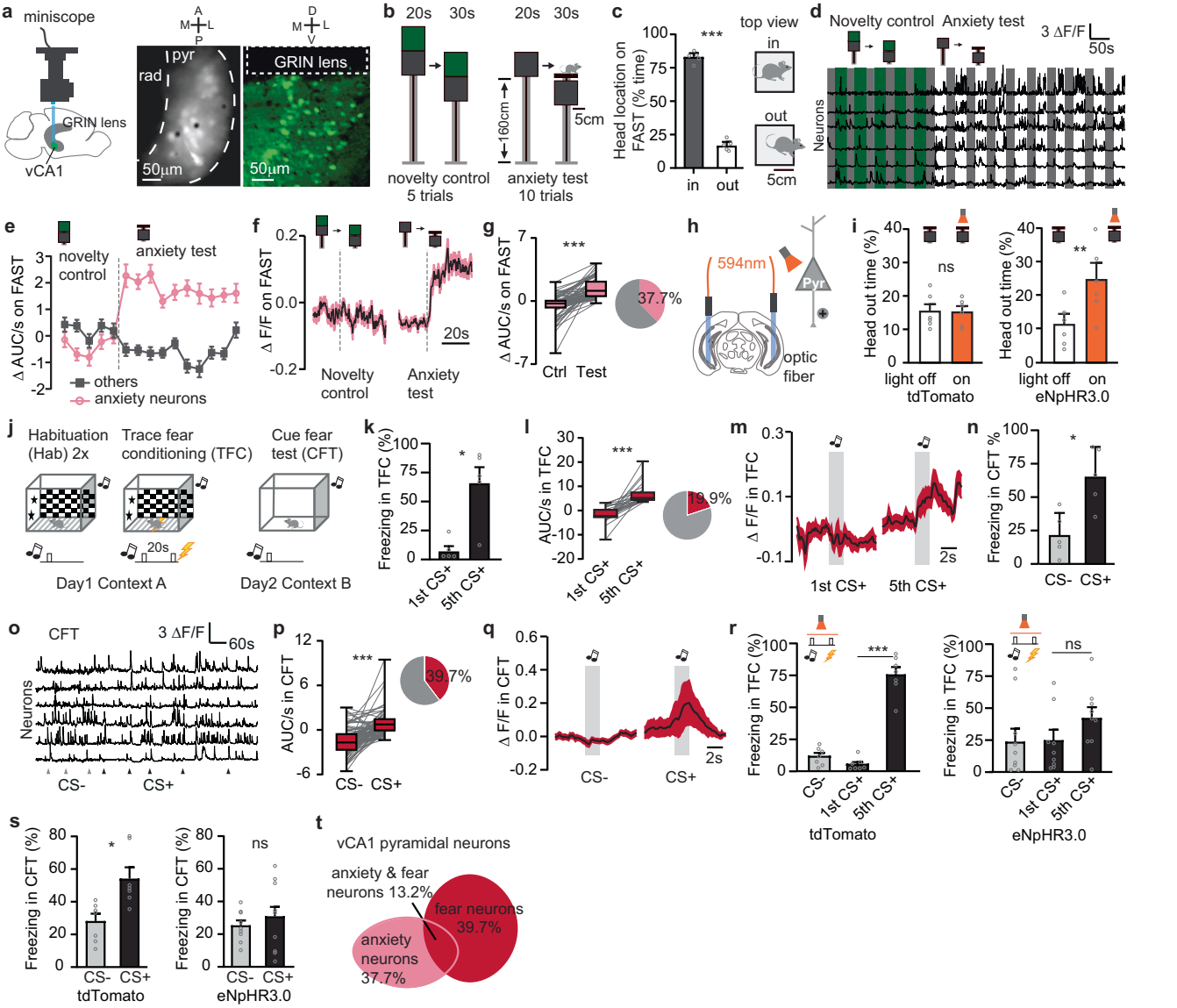

Fig. 1 | Distinct subpopulations of vCA1 pyramidal neurons represent anxiety and fear. a (Left) Schematic illustrating in vivo one-photon Ca^{2+} imaging of vCA1 pyramidal neurons with a miniscope. Sample images of GCaMP6f expressing pyramidal neurons acquired by miniscope in vivo (middle) and confocal imaging in situ (right). **b** Schematic of forced anxiety shifting task (FAST) protocol. **c** Head location time of C57BL/6 J mice on the FAST platform during anxiety test trials. $n = 5$ mice. **d** Sampled Ca^{2+} traces of pyramidal neurons during novelty control and anxiety test trials on FAST. **e** Mean activity ± SEM of anxiety and other neurons per trial. The FAST protocol consists of 5 sequential novelty control trials and 10 anxiety test trials, separated by a dotted line in the diagram. **f** Mean activity ± SEM of anxiety neurons responding to dark green cubicle (novel context) and open compartment (anxiogenic context). Dotted lines indicate the moving down of the black cubicle. **e**, **f** Anxiety $n = 77$ neurons, others $n = 127$ neurons from 5 mice. **g** Fraction of anxiety neurons and their averaged activity across all trials in novelty control and anxiety test. $n = 77$ neurons, 5 mice. **h** Design of optogenetic manipulation of vCA1 pyramidal neurons. **i** Mice protrude head out of FAST platform for longer time after inhibition of pyramidal neurons. tdTomato $n = 6$ mice, eNpHR3.0 $n = 6$ mice. **j** Trace fear conditioning protocol. **k** Mice learn to associate CS+ with US by showing higher freezing level to 5th CS+ than 1st CS+ during trace fear conditioning. $n = 5$ mice. **l**, **m** CSup pyramidal neuron responses to 1st and 5th CS+ . $n = 30$ neurons, 5 mice. **n** Mice freezing to CS- and CS+ during cued fear test. $n = 5$ mice. **o** Sampled Ca^{2+} traces of pyramidal neurons during cued fear test. **p** A subpopulation of pyramidal neurons selectively responded to CS+ during cued fear test. **q** Mean responses ± SEM of fear pyramidal neurons. **p**, **q** $n = 81$ neurons, 5 mice. **r** Mice cannot learn to associate CS+ with US after inhibition of pyramidal neurons. **s** Mice freezing level during cued fear test. **r**, **s** tdTomato $n = 7$ mice; eNpHR3.0 n = 9 mice. **t** Diagram illustrating fractions of vCA1 pyramidal anxiety and fear neurons. $^*P < 0.05$; $^{**}P < 0.01$; $^{***}P < 0.001$; ns: not significant. For bar graphs, data are presented as mean ± SEM. For box plots, box shows median, 25th and 75th percentiles and whiskers represent minima and maxima. Statistical analyses are listed in Supplementary Table 1.

small, elevated and well-lit platform. On the FAST, mice exhibited anxiety-like behavior by hesitating to extend their heads beyond the platform (Fig. 1c). A subpopulation of vCA1 pyramidal neurons, accounting for 37.7% of the whole vCA1 pyramidal neuron population, consistently showed enhanced activity in the anxiety-inducing trials, distinct from their responses in novelty control trials (Fig. 1d–g). The enhanced activity in the open compartment of FAST was not caused by behavioral changes such as the speed or orientation (Supplementary Fig. 2). Similarly, vCA1 pyramidal neurons also responded to the anxiogenic compartments of the EPM (Supplementary Fig. 3a–g) and in the center zone of an open field test (Supplementary Fig. 3h-k), thereby corroborating the observations from the FAST. These data altogether point to a general recruitment of anxiety-related neurons in anxiogenic conditions across different anxiety behavioral paradigms, while task-specific recruitment of vCA1 anxiety neurons is also observed (Supplementary Fig. 4). Subsequently, we examined whether

the activity of vCA1 pyramidal neurons was necessary for different anxiety tasks. To achieve this, we used eNpHR3.0-mediated optogenetic inhibition of vCA1 pyramidal neurons (Fig. 1h and Supplementary Figs. 1a, 3l). This intervention resulted in increased time spent with their heads outside the FAST platform (Fig. 1i) and greater exploration of the open arms in the EPM (Supplementary Fig. 3m). Collectively, these findings confirm the involvement of vCA1 pyramidal neurons in anxiety-related behaviors.

Considering the implication of the ventral hippocampus in fear behavior[27,28], we asked whether the vCA1 neurons representing anxiety differed from those associated with fear behavior. To investigate this, we subjected the same cohort of mice to a trace fear conditioning protocol while monitoring the activity of vCA1 pyramidal neurons. Mice underwent a discriminative trace fear conditioning (TFC) paradigm, in which five presentations of an auditory tone (conditioned stimulus, CS+) were paired with aversive foot-shocks (unconditioned stimulus, US) interleaved with a 20-seconds trace interval (Fig. 1j). Five presentations of an unpaired white noise (CS-) were used as a control tone. Mice learned to associate the neutral tone CS+ with the aversive US leading to higher freezing levels to the 5th CS+ compared to the 1st CS+ during trace fear learning (Fig. 1k and Supplementary Fig. 3n). Concomitantly, we observed that vCA1 pyramidal neurons displayed an activation (CSup) or inhibition (CSdown) to the 5th CS+ than the 1st CS+ indicating of fear learning-induced neuronal plasticity (Fig. 1l, m and Supplementary Fig. 3o, p). On the next day, we examined cued fear retrieval by presenting CSs in a novel context. Mice showed a discriminative fear memory with higher freezing levels to the threat-predicting CS+ compared to the non-reinforced CS- (Fig. 1n). Strikingly, a subpopulation of vCA1 pyramidal neurons (39.7%) responded to the CS+ but not to the CS- (Fig. 1o–q). Using the same approach as in the anxiety paradigm, we optogenetically inhibited vCA1 pyramidal neurons during trace fear learning and found an impairment in fear learning (in the presence of light) and cued memory retrieval (in the absence of light) (Fig. 1r, s and Supplementary Fig. 3q, r). These findings validated the pivotal role of vCA1 pyramidal neurons as an essential substrate for trace fear conditioning. To examine the potential overlap between neurons associated with anxiety and those involved in fear, we conducted an alignment analysis of task-responsive vCA1 pyramidal neurons during both the FAST and the cued fear memory test. This analysis unveiled predominantly separate subpopulations of vCA1 pyramidal neurons activated in response to either anxiety- or fear-related behaviors (Fig. 1t). Similar separation of vCA1 neuronal subpopulations was also observed when comparing the overlap between responsive neurons in either the EPM or open field test with cued fear memory test (Supplementary Fig. 9a, e). These data suggest that there are distinct microcircuits existing in vCA1 involved in either anxiety or fear processing. This observation naturally raises the question of which mechanism supports the formation of task-specific pyramidal neurons.

Inhibition of vCA1 Sst interneurons is necessary for fear learning

To delve into the neuronal circuit mechanisms responsible for the observed functional differentiation of vCA1 pyramidal neurons during anxiety- and fear-related behaviors, our focus turned to distinct vCA1 GABAergic interneurons that provide inhibitory inputs to specific subcellular domains of pyramidal neurons[29–32]. Somatostatin (Sst) interneurons preferentially form inhibitory synapses onto distal dendrites of pyramidal neurons to gate incoming excitatory inputs from e.g., the CA3 or entorhinal cortex (EC)[33]. By using Cre-dependent expression of GCaMP6f in Sst interneurons, we were able to specifically monitor the activity of vCA1 Sst interneurons during anxiety- and fear-inducing behaviors (Fig. 2a and Supplementary Fig. 1b, 5). Only a small fraction of Sst interneurons responded to anxiety during FAST (22.8%) (Fig. 2b–d), while we observed a substantial proportion of Sst interneurons (62.9%) activated in the center zone of the EPM (Supplementary Figs. 6a–f). To understand these divergent response patterns on FAST and EPM, we designed an optical approach to bilaterally activate vCA1 Sst interneurons with the excitatory opsin ChrimsonR, while simultaneously imaging vCA1 pyramidal neuron activity via a dual-color miniscope[34] (Fig. 2e and Supplementary Fig. 1c). Optogenetic activation of Sst interneurons had no impact on anxiety behavior and pyramidal neuron activity during FAST (Fig. 2f, g), while it increased open arm exploration on the EPM by inhibiting the activity of vCA1 pyramidal neurons (Supplementary Fig. 6g–i). Taken together, this indicates that vCA1 Sst interneurons do not play a significant role in modulating anxiety when mice are forcefully exposed to anxiety-inducing situations (e.g., FAST). However, vCA1 Sst interneurons become actively involved in anxiety-related processes that depend on decision-making, such as approach-avoidance behavior, as observed in the EPM task.

During trace fear learning, we observed that nearly half of Sst interneurons displayed a plastic inhibitory response from the 1st to the 5th CS+ (Fig. 2h–j and Supplementary Figs. 6j, k). On the following day at cued fear memory test, mice froze more to the CS+ than CS- and an even larger fraction of Sst interneurons (68.4%) exhibited inhibitory responses to the CS+ (Fig. 2k–o, Supplementary Fig. 9b). We opted to optogenetically activate, rather than inhibit, Sst interneurons during trace fear conditioning to detect a learning impairment, as Sst interneuron inhibition may have led to unnoticeable effects due to the ceiling in freezing levels during conditioning. Optogenetic activation of Sst interneurons during trace fear conditioning resulted in a decreased level of fear learning (Fig. 2p, q and Supplementary Figs. 6l, m). This reduction in fear learning was further linked to impaired cued fear retrieval after memory consolidation (Fig. 2s). The disruption of fear conditioning was probably caused by an inhibition of vCA1 pyramidal neurons during US presentation (Fig. 2r). The fact that optogenetic activation of Sst interneurons affected pyramidal neuron population activity differently during fear conditioning than in FAST suggests that Sst interneurons impact pyramidal neuron activity in a state-dependent fashion. Of important note, the fraction of pyramidal neurons responding to CS+ during the cued fear memory test dropped dramatically from 48.4% in the control to 23.1% in the ChrimsonR group (Fig. 2t). In summary, these findings indicate that the disinhibition of vCA1 pyramidal neurons by Sst interneurons during fear conditioning plays a crucial role in regulating associative learning.

Activation of vCA1 VIP interneurons disinhibits pyramidal neurons and mediates fear learning

Which presynaptic input may mediate the CS+ -related inhibition of Sst interneurons during trace fear conditioning? To address this question, we performed monosynaptic retrograde rabies tracing from vCA1 Sst interneurons[35,36] and quantified presynaptic inputs from the other two major interneuron subclasses, i.e., vasoactive intestinal peptide (VIP) and parvalbumin (PV) interneurons[37]. Our investigation revealed that nearly 9% of the presynaptic inputs onto Sst interneurons stemmed from vCA1 VIP interneurons, a notably higher proportion compared to vCA1 PV interneurons (3.2%) (Figs. 3a, b). The remaining presynaptic inputs primarily originated from local vCA1 pyramidal neurons (Fig. 3b). There are also extra-hippocampal inputs targeting Sst interneurons, however, their somata are not residing in vCA1 and thus did not interfere with the local CA1 intrinsic connectivity mapping. The heightened connectivity observed between VIP and Sst interneurons could potentially establish a circuit motif designed to disinhibit pyramidal neurons in the vCA1. This mechanism involves VIP interneurons inhibiting Sst interneurons, which, in turn, leads to the disinhibition of pyramidal neurons, a pattern reported in various brain regions[38,39]. Next, we examined the activity of VIP interneurons in the different behavioral paradigms. Only small fractions of VIP interneurons were activated in the FAST (9%) (Figs. 3c–f) and EPM (9.8% were activated in the open arms) (Supplementary Figs. 7a-f). Optogenetic inhibition of

https://doi.org/10.1038/s41467-024-52466-4

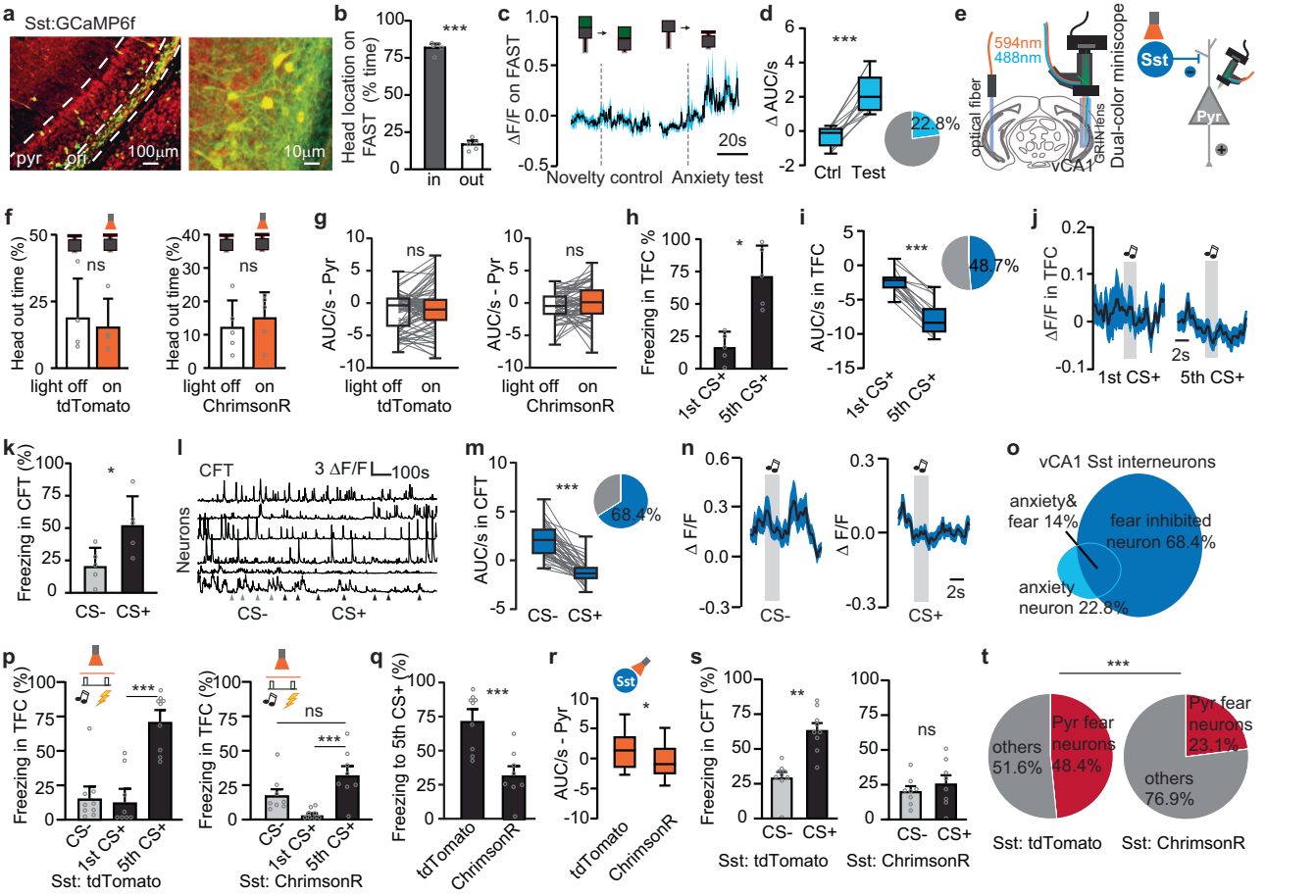

Fig. 2 | Inhibition of vCA1 Sst interneurons is necessary for fear learning. **a** Expression of GCaMP6f in vCA1 Sst interneurons. **b** Head location time of Sst mice on the FAST platform during anxiety test trials. $n = 5$ mice. **c** Mean responses ± SEM of Sst anxiety neurons to novelty control and anxiety tests on FAST. Dotted lines indicate the moving down of the black cubicle. **d** Fraction of Sst anxiety neurons and their activity pattern on FAST. **c**, **d** $n = 14$ neurons, 5 mice. **e** Design of dual-color miniscope and scheme of bilateral optogenetic activation of vCA1 Sst interneurons. **f** Optogenetic activation of Sst interneurons did not affect the head out time on FAST. tdTomato $n = 4$ mice, ChrimsonR $n = 5$ mice. **g** Optogenetic activation of Sst interneurons did not affect pyramidal neuron activity in anxiety test trials of FAST. tdTomato $n = 83$ neurons from 4 mice; ChrimsonR $n = 60$ neurons from 3 mice. **h** Sst mice freezing level to 1st and 5th CS+ during trace fear conditioning. $n = 5$mice. **i** Majority of Sst interneurons displayed CSdown responses to 5th CS+ as compared to the 1st CS+ .**j** Mean responses ± SEM to the 1st and 5th CS+ of CSdown Sst interneurons. **i**, **j** $n = 19$ neurons from 5 mice. **k** Sst mice freezing level to CSs during cued fear test. $n = 5$ mice. **l** Sampled Ca^{2+} traces of Sst interneurons during cued fear test. **m** Majority of Sst interneurons displayed inhibition to CS+ during cued fear test. **n** Mean CS- and CS+ responses ± SEM during cued fear test. **m**, **n** $n = 39$ neurons, 5 mice. **o** Diagram illustrating fractions of vCA1 Sst anxiety and fear interneurons. **p**, **q** Mice showed weaker associations between CS+ with US in ChrimsonR group during trace fear conditioning. tdTomato $n = 9$ mice; ChrimsonR $n = 8$ mice. **r** Dampened pyramidal neuron activity during US presentation in ChrimsonR group of mice. tdTomato $n = 63$ neurons, 4 mice; ChrimsonR $n = 105$ neurons, 3 mice. **s** Mice in ChrimsonR group did not consolidate cued fear memory. tdTomato $n = 9$ mice; ChrimsonR $n = 8$ mice. **t** Fractions of pyramidal neurons responding to CS+ during cued fear test. tdTomato $n = 91$ neurons, 4 mice; ChrimsonR $n = 117$ neurons, 3 mice. $^*P < 0.05$; $^{**}P < 0.01$; $^{***}P < 0.001$; ns: not significant. For bar graphs, data are presented as mean ± SEM. For box plots, box shows median, 25th and 75th percentiles and whiskers represent minima and maxima. Statistical analyses are listed in Supplementary Table 1.

VIP interneurons did not produce any noticeable changes in vCA1 pyramidal neuron activity or behavior during the FAST (Figs. 3g–j) or EPM (Supplementary Figs. 7g-i). In summary, these results indicate that vCA1 VIP interneurons are not crucial for anxiety-related behaviors.

However, during trace fear conditioning, a substantial proportion of VIP interneurons (41.9%) showed heightened activity to the 5th CS+ compared to the 1st CS+ (Figs. 3k–m and Supplementary Figs. 7j, k) indicating a plasticity mechanism that enables the association of conditioned cues with aversive stimuli. Moreover, even a higher fraction (57.6%) of VIP interneurons was activated to the CS+ during cued fear memory retrieval, providing further evidence of the active involvement of VIP interneurons in trace fear conditioning (Figs. 3n–q). After aligning neuronal identities during anxiety- and fear-related behaviors, we concluded that the majority of VIP interneurons was activated during fear- but not anxiety-related behavior (Fig. 3r, Supplementary Fig. 9c). Following up, we addressed whether VIP interneuron activation is essential to trace fear learning and subsequent memory retrieval. First, we observed a decrease in pyramidal neuron activity when VIP interneurons were inhibited (Fig. 3u). Next, through optogenetic inhibition of VIP interneurons during CS+ -US pairings, we noted a reduction in trace fear learning (Figs. 3s, t and Supplementary Figs. 7l, m), as well as an impairment in cued fear memory retrieval during testing on the following day (Fig. 3v). It is thus plausible that the inhibition of VIP interneurons led to the suppression of pyramidal neuron activity, potentially impeding the CS+ -related plasticity during trace fear learning, since a smaller fraction of pyramidal neurons responded to the CS+ during fear retrieval in the VIP optogenetic inhibition group compared to the control (Fig. 3w). Collectively, these findings strongly suggest a functional relationship between VIP interneurons and pyramidal neurons during trace fear

https://doi.org/10.1038/s41467-024-52466-4

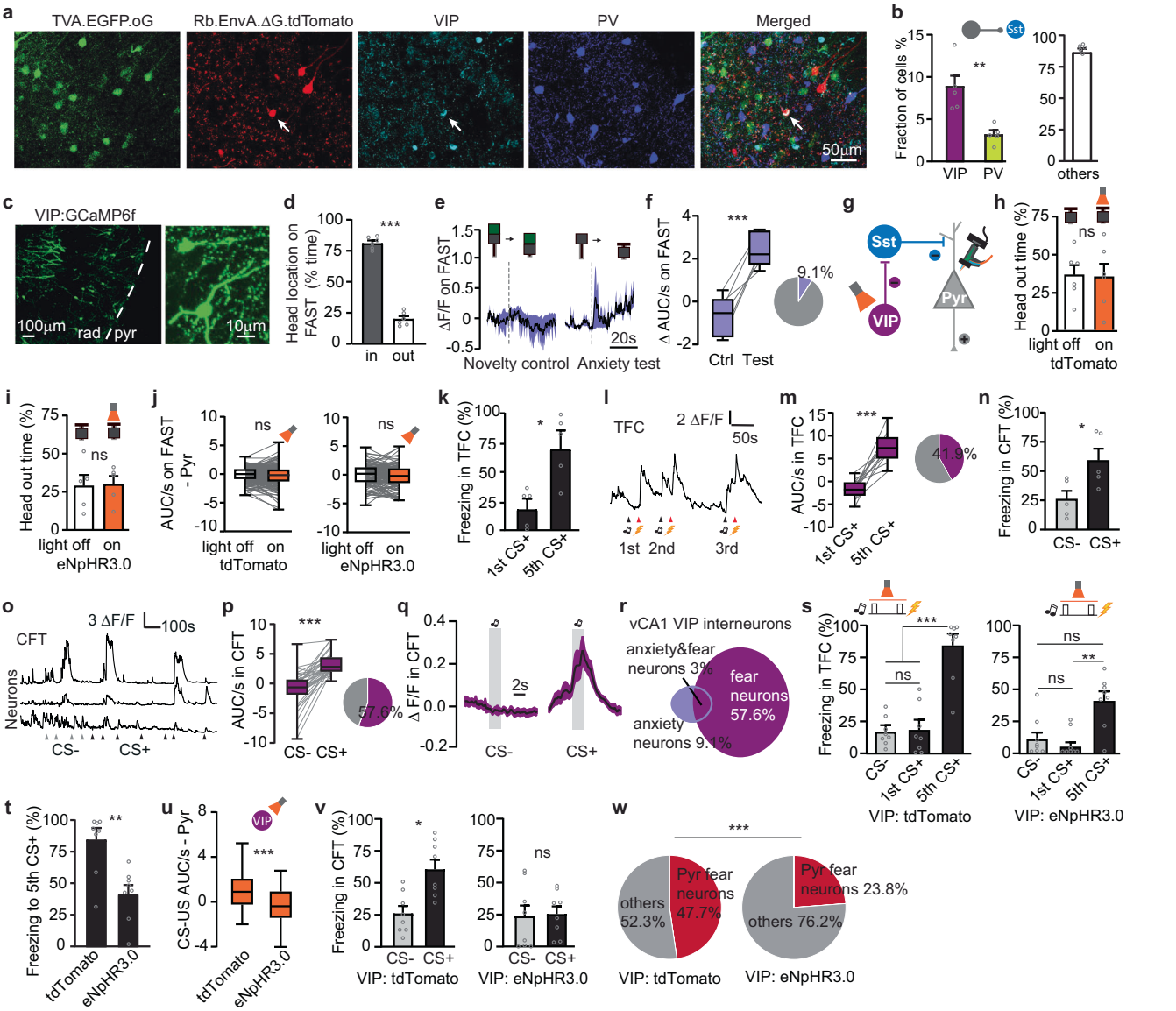

Fig. 3 | Activation of vCA1 VIP interneurons disinhibits pyramidal neurons and mediates fear learning. **a** Sampled maximum projection images of presynaptic input cells to vCA1 Sst interneurons. Arrowhead indicates the co-localization of tdTomato and VIP antibody conjugated fluorescence. **b** Bar graph showing the percentage of presynaptic neurons to vCA1 Sst interneurons. $n = 1068$ tdTomato+ cells from 5 mice. **c** Expression of GCaMP6f in vCA1 VIP interneurons. **d** Head location time of VIP mice on the FAST platform during test trials. $n = 6$ mice. **e** Mean responses ± SEM of VIP anxiety neurons responding to novelty control and anxiety tests on FAST. Dotted lines indicate the moving down of black cubicle. **f** Fraction of VIP anxiety neurons and their activity during novelty controls and anxiety tests. **e**, **f** $n = 6$ neurons, 6 mice. **g**–**i** Optogenetic inhibition of VIP interneurons did not affect the head out time on FAST. tdTomato $n = 6$ mice; eNpHR3.0 $n = 5$ mice. **j** Optogenetic inhibition of VIP interneurons did not affect pyramidal neuron activity in test trials of FAST. tdTomato $n = 129$ neurons, 3 mice; eNpHR3.0 $n = 190$ neurons, 3 mice. **k** VIP mice freezing level to 1st and 5th CS+ during trace fear conditioning. $n = 5$ mice. **l** Sample Ca^{2+} trace of a VIP interneuron in trace fear conditioning. **m** Majority of VIP interneurons displayed CSup responses to 5th CS+ in trace fear conditioning. $n = 13$ neurons, 4 mice. **n** VIP mice freezing level to CSs in cued fear test. $n = 5$mice. **o** Sampled Ca^{2+} traces of VIP interneurons during cued fear test. **p** Majority of VIP interneurons were activated to CS+ during cued fear test. **q** Mean CS- and CS+ responses ± SEM of VIP fear interneurons during fear test. **p**, **q** $n = 38$ neurons, 6 mice. **r** Fractions of VIP anxiety and fear interneurons. **s**,**t** Mice in eNpHR3.0 group showed weaker associations between CS+ and US. tdTomato $n = 8$ mice; eNpHR3.0 $n = 8$ mice. **u** Dampened pyramidal neuron activity during CS-US presentation in eNpHR3.0 group of mice. tdTomato $n = 149$ neurons from 3 mice; eNpHR3.0 $n = 163$ neurons from 3 mice. **v** Mice in eNpHR3.0 group did not consolidate cued fear memory. tdTomato $n = 8$ mice; eNpHR3.0 $n = 8$ mice. **w** Fractions of pyramidal neurons responding to CS+ during cued fear test. tdTomato $n = 172$ neurons from 3 mice; eNpHR3.0 $n = 181$ neurons from 3 mice. $^{*}P < 0.05$; $^{**}P < 0.01$; $^{***}P < 0.001$; ns: not significant. For bar graphs, data are presented as mean ± SEM. For box plots, box shows median, 25th and 75th percentiles and whiskers represent minima and maxima. Statistical analyses are listed in Supplementary Table 1.

conditioning, presumably mediated through Sst interneurons. This inference is supported by the parallel activity patterns of VIP interneurons during trace fear learning and memory retrieval, which align with those of pyramidal neurons (CS+ -related activation), while demonstrating a contrasting pattern compared to Sst interneurons (CS+ -related inhibition).

vCA1 PV interneurons are involved in anxiety

PV interneurons, a prominent population of GABAergic interneurons in the vCA1, are known as fast-spiking, highly active neurons that provide powerful feedback and feedforward inhibition to different spatial domains of pyramidal neurons, with a preference for targeting their perisomatic region[40]. Research has shown their crucial role in

https://doi.org/10.1038/s41467-024-52466-4

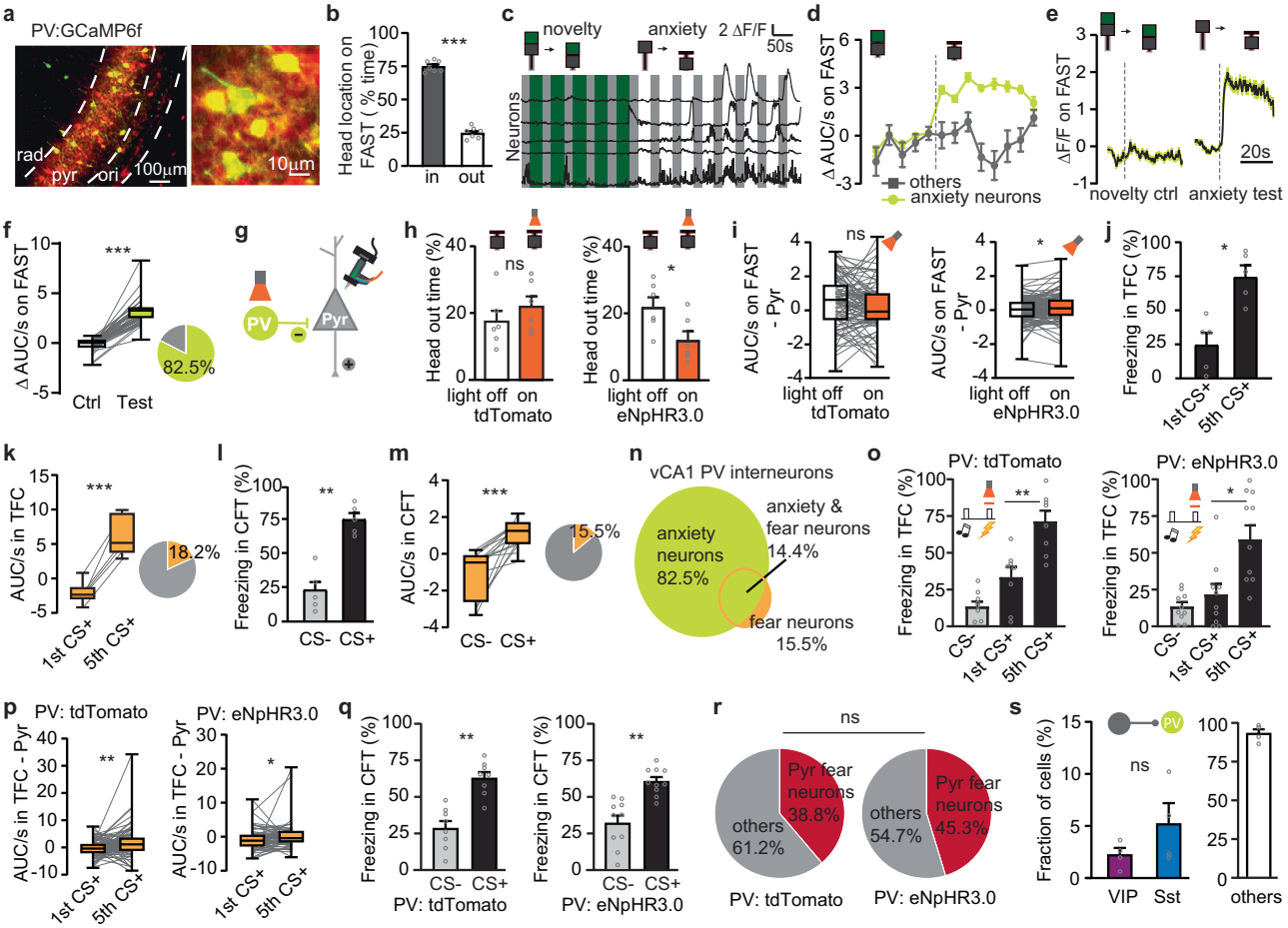

Fig. 4 | vCA1 PV interneurons are involved in anxiety. a Expression of GCaMP6f in vCA1 PV interneurons. **b** Head location time of PV mice on the FAST platform during anxiety test trials. $n = 7$ mice. **c** Sampled Ca^{2+} traces of PV interneurons during novelty control and anxiety test trials on FAST. **d** Mean activity of anxiety neurons and non-responding neurons per trial. Dotted line separates sequentially 5 novelty trials and 10 anxiety test trials. **e** Mean responses ± SEM of PV anxiety interneurons responding to novelty control and anxiety tests on FAST. Dotted lines indicate the moving down of the black cubicle. **d**, **e** Anxiety neurons $n = 60$ neurons, others $n = 17$ neurons from 6 mice. **f** Fraction of PV anxiety interneurons and their activity during novelty controls and anxiety tests. $n = 80$ neurons from 6 mice. **g**, **h** Optogenetic inhibition of PV interneurons decreased head out time on FAST. tdTomato $n = 6$ mice; eNpHR3.0 $n = 6$ mice. **i** Optogenetic inhibition of PV interneurons disinhibited pyramidal neuron activity in anxiety test trials of FAST. tdTomato $n = 89$ neurons from 2 mice; eNpHR3.0 $n = 125$ neurons from 4 mice. **j** PV mice freezing level to 1st and 5th CS+ during trace fear conditioning. $n = 5$ mice. **k** Small proportion of PV interneurons responded to 5th CS+ in trace fear conditioning. $n = 6$ neurons, 6 mice. **l** PV mice freezing level to CSs in cued fear test. $n = 5$ mice. **m** Small proportion of PV interneurons were activated to CS+ during cued fear test. $n = 15$ neurons, 6 mice. **n** Fractions of PV anxiety and fear interneurons. **o** Optogenetic inhibition of PV interneurons in trace fear conditioning had no effect on trace fear learning. tdTomato $n = 8$ mice; eNpHR3.0 $n = 10$ mice. **p** Optogenetic inhibition of PV interneurons during trace fear conditioning did not affect pyramidal neuron responses to 5th CS+ . tdTomato $n = 89$ neurons from 2 mice; eNpHR3.0 $n = 66$ neurons from 5 mice. **q** Mice in eNpHR3.0 group showed high freezing to CS+ in cued fear test. tdTomato $n = 8$ mice; eNpHR3.0 $n = 10$ mice. **r** Fractions of pyramidal fear neurons responding to CS+ during cued fear test. tdTomato $n = 121$ neurons from 2 mice; eNpHR3.0 $n = 150$ neurons from 5 mice. **s** Bar graph showing the percentage of presynaptic neurons to vCA1 PV interneurons. $n = 1281$ tdTomato+ cells from 4 mice. $^*P < 0.05$; $^{**}P < 0.01$; $^{***}P < 0.001$; ns: not significant. For bar graphs, data are presented as mean ± SEM. For box plots, box shows median, 25th and 75th percentiles and whiskers represent minima and maxima. Statistical analyses are listed in Supplementary Table 1.

social memory formation and anxiety within the vCA1 circuitry[41,42]. Yet, whether vCA1 PV interneurons are differentially involved in anxiety or fear has not been investigated thus far.

PV interneurons were robustly activated in the anxiogenic compartment of FAST (Figs. 4a–f) and EPM (Supplementary Fig. 8a–g). Optogenetic inhibition of PV interneurons increased anxiety in mice as indicated by shorter 'head-out' time on the FAST platform (Figs. 4g,h) and less exploration of the open arms of the EPM (Supplementary Fig. 8h). The enhanced anxiety was associated with the disinhibition of vCA1 pyramidal neurons during optogenetic inhibition of PV interneurons (Fig. 4i and Supplementary Fig. 8i). In contrast to anxiety, most PV interneurons did not respond to the CS+ during trace fear learning and retrieval (Figs. 4j–m and Supplementary Figs. 8j, k). The analysis of the overlap between PV interneuron responsiveness to FAST and cued fear memory retrieval indicated that PV interneurons are primarily activated during anxiety- but not fear-related behavior (Fig. 4n, Supplementary Fig. 9d). Given that PV interneurons rarely responded to CS+ but did show noticeable responses to the US (Supplementary Fig. 8l), we investigated the role of PV interneuron activity in trace fear learning by optogenetically inhibiting them during US presentations. Strikingly, the inhibition of PV interneurons did not affect trace fear learning and retrieval (Figs. 4o, q and Supplementary Figs. 8m–o), as pyramidal neurons continued to exhibit CS+ -related plastic changes during trace fear learning (Fig. 4p) and reliably responded to the CS+ during cued fear memory retrieval (Fig. 4r). The notion that PV interneurons do not play a role in trace fear conditioning was further supported by their limited connectivity to VIP (2.3%) and Sst (5.3%) interneurons, contrasted by enriched presynaptic

inputs originating from PV interneurons themselves as reported previously[31,43] (Fig. 4s). In summary, these results indicate that vCA1 PV interneurons primarily modulate the activity of vCA1 pyramidal neurons to regulate anxiety, without impacting trace fear conditioning.

Discussion

Using longitudinal in vivo Ca^{2+} imaging and optogenetic manipulations of vCA1 pyramidal neurons and subclasses of GABAergic interneurons, we discovered a division of labor in inhibitory microcircuits during anxiety- and fear-related behaviors. VIP and Sst interneurons form a microcircuit that dis-inhibit a subpopulation of pyramidal neurons during fear (*'the vCA1 fear microcircuit'*), while PV interneurons targeting a distinct subpopulation of pyramidal neurons regulate anxiety (*'the vCA1 anxiety microcircuit'*).

Within the vCA1 fear microcircuit, the disinhibitory VIP-Sst-Pyr circuit motif appears to function as a gateway that enables excitatory inputs to reach pyramidal neurons, facilitating the formation of associations between conditioned cues and unconditioned stimuli. A sparse population of pyramidal neurons has been demonstrated to be activated by both the conditioned stimulus (CS+) and the unconditioned stimulus (US), contributing to the formation of neural assemblies that underlie memory engrams[44–46]. Sst interneurons play a pivotal role in inhibiting a large fraction of pyramidal neurons during US presentation, leaving only a small subpopulation of pyramidal neurons activated and recruited to form the memory engram[47]. In the context of trace fear conditioning within the vCA1 region, our findings revealed that Sst interneurons are inhibited upon the presentation of the conditioned stimulus (CS+), leading to an heightened activity of a specific subpopulation of pyramidal neurons, that may facilitate the formation of the association between the CS+ and US. The inhibition of Sst interneurons is likely mediated by local VIP interneurons[38,39,48], since VIP interneurons exhibited a preferential connectivity to Sst interneurons and an opposite activity pattern in the form of an excitation in response to the CS+ . Of note, brainstem nucleus incertus GABAergic neurons have been shown to selectively inhibit hippocampal Sst interneurons and may therefore also contribute to the fine-tuning of pyramidal neuron activity during the formation of contextual fear memories[49]. The activity patterns of VIP and Sst interneurons, and the CS+ -activated pyramidal neurons, remained consistent throughout both trace fear learning and memory retrieval. This consistency suggests that fear memories are encoded in the vCA1 region with remarkable stability and precision. Notably, Sst interneurons were also found to be engaged during anxiety-related behaviors, with their recruitment contingent on the specific task demands. During the forced anxiety-inducing task (FAST), Sst interneurons exhibited limited activation. However, they played a more prominent role in the center zone of the elevated plus maze (EPM), a task involving decision-making processes. This observation suggests a flexible and state-dependent role for vCA1 Sst interneurons in modulating anxiety, extending beyond their involvement in associative fear learning.

When animals encounter anxiety-inducing situations, vCA1 pyramidal neurons become activated, conveying relevant information to the lateral hypothalamus and medial prefrontal cortex to orchestrate anxiety responses[18,19]. In the vCA1 anxiety microcircuit, the activation of pyramidal neurons can be 'set' at an appropriate level by perisomatic inhibition provided by PV interneurons. This mechanism likely plays a role in adaptively adjusting anxiety levels by modulating the activity of pyramidal neurons that control anxiety responses[12]. In line with this concept, optogenetic inhibition of PV interneurons resulted in the 'over-activation' of pyramidal neurons via a dis-inhibitory process, leading to heightened anxiety levels, as evidenced by reduced exploration of anxiogenic environments. PV interneurons can inhibit pyramidal neuron activity through both feedback and feedforward mechanisms[40,50], and under the influence of cholinergic modulation from medial septum or serotoninergic modulation from the raphe nuclei[51–53]. Therefore, we speculate that neuromodulatory inputs may be crucial in regulating the degree of activation within the vCA1 anxiety microcircuit, ultimately influencing anxiety levels.

The GABAergic Cre mouse lines provided genetic access to study PV, Sst or VIP interneuronal subclasses, however, 'masked' the specific identities of the nearly 30 GABAergic cell-types of the complex CA1 circuitry[29,31,36]. Thus, further tools and techniques are needed to dissect the contributions of different GABAergic cell-types to emotional behavior. Hippocampal GABAergic Sst cells consist of oriens/lacunosum-moleculare (OLM) cells and bistratified cells as well as of back-projecting and double-projecting cells. While OLM cells provide inhibition onto distal dendrites of pyramidal neurons, fast-spiking bistratified cells provide recurrent inhibition to basal and proximal apical dendrites of pyramidal neurons[54,55]. We observed that 68.4% of vCA1 Sst interneurons are inhibited during fear learning, with a persistent inhibition at fear memory retrieval. We speculate that fear-inhibited vCA1 Sst interneurons may correspond to OLM cells which control the information flow onto pyramidal neurons from input brain regions such as the CA3 or EC[33,56]. Besides, a minor proportion of Sst interneurons was activated in anxiety. This population might correspond to bistratified cells since they co-express PV, a marker predicting strong activation in our anxiety tasks. VIP interneurons in the CA1 hippocampus have been categorized as interneuron-specific cells constituting around 8.3% of all interneurons and VIP expressing basket cells constituting about 1% of all interneurons[35]. Given the strong inhibition of Sst interneurons concomitant with the activation of VIP interneurons, we hypothesize that fear responding VIP interneurons may correspond to interneuron-specific cells that preferentially innervate OLM cells[57]. In contrast to their strong recruitment during fear learning and retrieval, only a small proportion of VIP interneurons responded to anxiety and thus may speculatively correspond to VIP expressing basket cells. Lastly, because a large fraction of PV interneurons (up to 82.5%) were activated during anxiety behaviors, we speculate that these PV cells may be composed of major PV GABAergic cell-types of the CA1 microcircuit such as basket cells, axo-axonic cells or bistratified cells[36].

Our study reinforced the importance of a disinhibitory circuit mechanism mediated by VIP and Sst interneurons for associative learning. During fear learning, pyramidal neurons receive salient signals from e.g., the CA3 and EC that are instrumental to drive synaptic plasticity[47,58]. In parallel, VIP interneurons also receive inputs from the CA3 and EC, as well as from local pyramidal neurons in the CA1 hippocampus[59]. In the vCA1 fear microcircuit, the VIP disinhibitory circuit probably amplifies or gates pyramidal neuron activity through firstly feed-forward excitation received from the CA3 and EC inputs and secondly via local feed-back excitatory circuits received by vCA1 pyramidal neurons that may provide further excitation to vCA1 VIP interneurons.

Previous studies revealed long-range projections originating from or projecting to the ventral hippocampus differentially involved in anxiety- and fear-related behavior. Particularly, the projection pathways from the vCA1 to subnuclei of the amygdala, including the central amygdala (CeA), basolateral amygdala (BLA) as well as basal amygdala (BA), play a role in contextual fear learning (vCA1→BLA), contextual fear memory retrieval (vCA1→BA) and context-dependent cue fear memory retrieval (vCA1→CeA)[13,21,22]. The ventral hippocampus also controls the expression of fear after conditioning via projection to interneurons in the prelimbic cortex (vH→PrL)[16]. Moreover, the vCA1 also receives long-range projection inputs from the entorhinal cortex (EC→vCA1) during trace fear learning to form temporal association memory[60], and basolateral amygdala (BLA→vCA1) to support fear extinction memory[61]. In addition to fear learning and expression, the ventral hippocampus also plays a crucial role in anxiety-related behavior. vCA1 modulates anxiety behaviors through projections to the medial prefrontal cortex (vCA1→mPFC)[8,18,20,62,63], lateral septum

https://doi.org/10.1038/s41467-024-52466-4

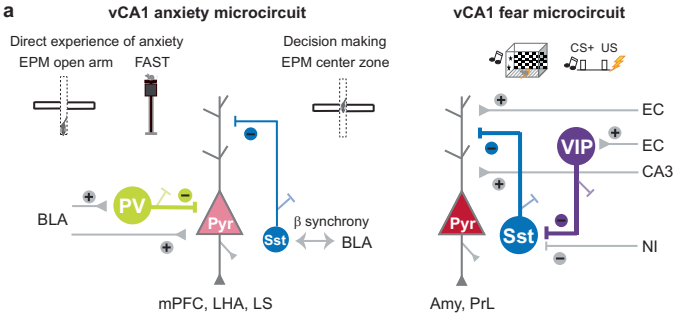

b

vCA1 neurons	TFC	FAST	EPM
Pyr neurons	Activated	Activated	Activated
Pyr inhibition	Impairs fear learning	Reduces anxiety	Reduces anxiety
Sst interneurons	Inhibited	×	Activated
Sst activation	Impairs fear learning	no effect	Reduces anxiety
VIP interneurons	Activated	×	×
VIP inhibition	Impairs fear learning	no effect	no effect
PV interneurons	×	Activated	Activated
PV inhibition	no effect	Increases anxiety	Increases anxiety

Fig. 5 | vCA1 inhibitory microcircuits for anxiety and fear. a Schematic overview of vCA1 anxiety and fear microcircuits. In the vCA1 anxiety microcircuit, PV and anxiety pyramidal neurons represent the direct experience of anxiety i.e., in the open arms of the EPM and high platform of the FAST. Moreover, Sst interneurons are predominantly activated in the center zone of the EPM, suggesting a role in the decision making during approach-avoidance behavior. In the vCA1 fear microcircuit, VIP and Sst interneurons mediate trace fear learning and retrieval via disinhibition of fear pyramidal neurons. BLA: basolateral amygdala; mPFC: medial prefrontal cortex; LHA: lateral hypothalamus area; LS: lateral septum; Amy: amygdala; PrL: prelimbic cortex; EC: entorhinal cortex; NI: nucleus incertus. **b** Table summarizes activity patterns and the impact of optogenetic manipulations in the 4 major vCA1 neuronal subclasses tested during anxiety and fear behavioral paradigms. The cross indicates that a neuronal subclass was not required for a particular behavioral task.

(vCA1→LS)[64], and lateral hypothalamus (vCA1→LH)[19], as well as via β synchrony and monosynaptic inputs from BLA (BLA→vCA1)[10,65]. These intricate projection pathways closely interact with one another, yet largely convey task-specific information. CA1 inhibitory interneurons may shape such task- and projection-specific activity via biased functional connectivity motifs with CA1 pyramidal neurons[60,66]. Therefore, we infer that the *'vCA1 fear inhibitory microcircuit'* likely interfaces predominantly with vCA1 projections targeting the amygdala and prelimbic cortex, whereas the *'vCA1 anxiety inhibitory microcircuit'* is anticipated to modulate the activity of vCA1 projections to the medial prefrontal cortex, lateral hypothalamus and lateral septum (Fig. 5).

Our results revealed the intricate neuronal microcircuitry within the vCA1 underlying the processing of two distinct negative emotions: anxiety and fear. The vCA1 region functions as a central hub, orchestrating responses to both anxiety and fear-related behavior, by integrating signals from distant brain regions associated with emotions[61] and leveraging the activity of distinct GABAergic interneurons and projection neurons. Such complex and dynamic circuit organization allows animals to promptly evaluate and react to diverse threats, promoting learning processes, such as in the case of fear conditioning, or the execution of innate behaviors, as observed in anxiety. This adaptability proves essential, particularly when threats exhibit variations in quality, proximity, intensity, or the probability of occurrence[2]. Our discoveries offer insights into how dysfunctional inhibitory microcircuits within the hippocampus may contribute to disorders related to anxiety and fear[67].

Methods

Animals

Mice aged 3 to 6 months were group housed with ad libitum access to food and water on a 12-hour light/dark cycle at constant temperature (22 ± 1 °C) and humidity (30–40%). C57BL/6 J mice (Janvier Labs, France), PV-IRES-Cre (Jackson Laboratory, Strain #008069), Sst-IRES-Cre (Jackson Laboratory, Strain #013044), VIP-IRES-Cre (Jackson Laboratory, Strain #010908) mice of both sexes were used in this study[68,69]. These transgenic mouse lines are of B6 background and had been backcrossed with C57BL/6 J wild type mice for more than ten generations to produce heterozygous offspring with B6J congenic background. Only heterozygous mice were used for experiments.

Following surgery, mice undergoing in vivo Ca^{2+} imaging experiments were single-housed to secure miniscope implantation. For optogenetic manipulation and rabies tracing experiments, littermates were randomly assigned to experimental conditions and group-housed with two to four mice per cage. All experimental procedures were performed in accordance with the guidelines of the Animal Welfare Office at the University of Bern and approved by the Veterinary Office of the Canton of Bern.

Surgery

Mice were anesthetized with isoflurane (induction 3%, maintenance 1.5%) in oxygen at a flow rate of 1 L/min throughout the procedure. Core body temperature was kept at 37 °C by a feed-back controlled heating pad (Harvard Apparatus, Germany). Ophthalmic cream was applied to avoid eye drying. Local analgesia was applied by injecting a mixture of 2% of lidocaine (Streuli Pharma, Switzerland) and 0.5% bupivacaine (Aspen Pharma, Switzerland) subcutaneously under the scalp. Anesthesia depth was confirmed by detecting deep breathing and lack of toe pinch reflex. After mice were mounted onto a stereotaxic frame (David Kopf Instruments, USA), the scalp was incised and craniotomies were made over target regions. The surgical opening on skull is about Ø 0.1 mm for rabies tracing experiments, Ø 0.3 mm for optical fiber implantation and Ø 0.7 mm for gradient-index (GRIN) micro lens implantation. Mice were given additional analgesia for 3 days after operation (carprofen, 5 mg/kg subcutaneously). Implants e.g., optical fibers and GRIN lenses were secured to the skull using light-cured dental adhesive (Kerr, OptiBond Universal) and dental cement (Ivoclar, Tetric EvoFlow).

Virus injection and GRIN lens implantation for miniscope. Conditional GCaMP6f viruses were injected into the mouse brain with the following coordinates: AP −3.28 mm, ML + 3.45 mm, DV −4.0 mm relative to bregma. 250 nL viral solution was delivered via a glass micropipette (about Ø 20 µm at tip) attached by a tubing to a Picospritzer III microinjection system (Parker Hannifin Corporation) at a speed of 20 nL per minute. For labeling of pyramidal neurons, AAV1.CaMKII.GCaMP6f virus (Addgene #100834, titer 2.3×10^{13} vg/mL, dilution 1:3 for injection) was used in C57BL/6 J mice. For labeling of PV, Sst or VIP interneurons, AAV5.Syn.Flex.GCaMP6f (Addgene #100833, titer 7×10^{12} vg/mL) was used in combination with each GABAergic Cre mouse lines.

After infusion of viruses, the glass micropipette was kept in place for 40–60 min to prevent viral solution backflow. Then the glass pipette was slowly retracted. The needle endomicroscope GRIN lens (Ø 0.6 mm) was slowly lowered to DV −4.0 mm at a speed of 0.5 mm per minute by using a leading 21 gauge needle attached to a custom-made stereotaxic guide enabling precise placement of the lens. The lens was fixed to the skull surface with light-cured dental adhesive and dental cement. The surface of the skull was made coarse by scratching with blade or gentle drilling to increase the adhesion with dental cement. Three skull screws were inserted around the implantation site and cemented together with the GRIN lens to ensure the implant's stability.

Additional cement was placed around the lens to form a well-shape cave to protect lens edge from damage.

From the third week post virus injection, GCaMP6f expression was inspected several times over consecutive weeks. Mice with good virus expression were fixed in a stereotaxic frame under isoflurane anesthesia to attach an aluminum baseplate for miniscope (UCLA, V3) above the GRIN lens. After finding the best field of view, the baseplate was cemented onto the skull and a plastic cap was used to protect the GRIN lens from dust. Mice wore a dummy miniscope for 2 weeks to adapt to the additional weight on head before behavioral tests and Ca^{2+} signal imaging.

Virus injection and fiber implantation for optogenetic manipulation experiments. For bilateral optogenetic manipulation experiments, viruses encoding the inhibitory opsin eNpHR3.0 or excitatory opsin ChrimsonR, or a control tdTomato were injected at the following coordinates: AP −3.15 mm, ML ± 3.0 mm, DV −4.5 mm relative to bregma. These coordinates are slightly different from the miniscope setting because the small size of optical fiber (Ø 0.2 mm) allowed us to penetrate deeper into the ventral hippocampus without too much damage to hippocampal structures. For the inhibition of pyramidal neurons, 400 nL AAV5-CaMKIIα-eNpHR3.0-mCherry virus (UNC Vector Core, titer 5.8×10^{12} vg/mL) was used in C57BL/6 J mice. 400 nL AAV2-CaMKIIα-mCherry virus (UNC Vector Core, titer 4.7×10^{12} vg/mL) was used as control. For the inhibition of VIP and PV interneurons, 500nL AAV1-hEF1α-dlox-eNpHR3.0-iRFP-dlox virus (ETH Zurich Viral Vector Facility, v203, titer 3.8×10^{12} vg/mL) was used in either VIP-IRES-Cre or PV-IRES-Cre mouse line. 400 nL AAV8-EF1α1.1-Flex-tdTomato virus (UNC Vector Core, 4.5×10^{12} vg/mL) was used as control. For excitation of Sst interneurons, 400nL AAV1-hSyn1-dlox-ChrimsonR-tdTomato-dlox (ETH Zurich Viral Vector Facility, v289, titer 4.9×10^{12} vg/mL) was used in Sst-IRES-Cre mouse line. 400 nL AAV8-EF1α1.1-Flex-tdTomato virus was used as control. After injection, the glass micropipette was left in place for another 20 min and then withdrawn slowly.

Optical fibers (200 µm core, 0.37 NA; Thorlabs) were cleaved to the appropriate length and secured to ceramic ferrules (Ø 230 µm bore, Senko) with tiny epoxy glue. After retracting glass micropipette, the optical fibers were attached into a stereotaxic cannula holder (Doric Lenses, Canada) and slowly inserted into the brain tissue at the same coordinate of virus injection.

Virus injection and fiber and GRIN lens implantation for dual-color miniscope. For dual-color miniscope imaging experiments, the GRIN lens was implanted into the right hemisphere of the ventral hippocampus and the optical fiber on the left. The virus injection coordinates, fiber or GRIN lens implantation were the same as described in the above sections. For dual-color miniscope imaging of pyramidal neurons while inhibiting VIP or PV interneurons, a mixture of 100 nL AAV1.CaMKII.GCaMP6f and 400 nL AAV1-hEF1α-dlox-eNpHR3.0-iRFP-dlox was injected into the right hemisphere of the ventral hippocampus (AP −3.28 mm, ML + 3.45 mm, DV −4.0 mm) and 500 nL AAV1-hEF1α-dlox-eNpHR3.0-iRFP-dlox into the left hemisphere of the ventral hippocampus (AP −3.15 mm, ML ± 3.0 mm, DV −4.5 mm). For dual-color miniscope imaging of pyramidal neurons while activating Sst interneurons, a mixture of 100 nL AAV1.CaMKII.GCaMP6f and 400 nL AAV1-hSyn1-dlox-ChrimsonR-tdTomato-dlox was injected into the right hemisphere of the ventral hippocampus (AP −3.28 mm, ML 3.45 mm, DV −4.0 mm) and 500 nL AAV1-hSyn1-dlox-ChrimsonR-tdTomato-dlox into the left hemisphere of the ventral hippocampus (AP −3.15 mm, ML −3.0 mm, DV −4.5 mm). For controls, 400 nL AAV8-EF1α1.1-Flex-tdTomato was injected together with AAV1.CaMKII.GCaMP6f.

After virus injection, 2 skull screws were fixed at a position anterior to the bregma. An optical fiber was first implanted into the left hemisphere and secured with dental adhesive, and then the GRIN lens into the right hemisphere according to the procedure described in the above section. Dental cement was applied to secure screws, fiber and GRIN lens onto the skull. Mice were then returned to the animal facility and housed individually. 10 days of postoperative care and 3 days of analgesia were provided to these mice.

Rabies tracing. In order to investigate the presynaptic input neurons to Sst or PV interneurons, retrograde rabies tracing was performed in Sst-IRES-Cre or PV-IRES-Cre mice. First, 200 nL viral solution containing the AAV2/9-hSyn1-DIO-TVA950-2A-EGFP-2A-oG (ETH Zurich Viral Vector Facility) was injected into the ventral hippocampus at the following coordinates: AP-3.25 mm, ML ± 3.45 mm and DV −4.0 mm. After suturing the scalp incision, mice were returned to their home cage and colony room. 2 weeks later, mice underwent a second surgery during which 150 nL recombinant rabies virus EnvA-N2C-RVdG-tdTomato (Kavli Institute for Systems Neuroscience Viral Vector Core, Norwegian University of Science and Technology) was infused into the ventral hippocampus at the same coordinates as above. After 5-6 days, mice were sacrificed and their brains were harvested.

Behavior

The mice were habituated to the room and the testing chamber for at least 3 days before behavior test by placing mice in home cage into the testing chamber for 2 × 30 min daily. Each mouse had its own custom-made nesting house made of hard paper, which was used for transferring mice to testing apparatus to reduce mouse grabbing. The mice were also habituated to be moved out of the home cage many times prior to experiments.

Forced Anxiety Shifting Task (FAST). The FAST paradigm is a trial-based anxiety behavioral task consisting of an elevated platform (160 cm from the ground, 10 cm×10 cm) surrounded by a motorized black cubicle (11 cm × 11 cm). The FAST has been developed by Konstantinos Koukoutselos as an integral part of his PhD thesis ('Anticipatory coding of anxiety in the ventral hippocampus', 2023, University of Bern, Switzerland, manuscript in preparation)[26]. Mice were placed on top of the platform inside the black cubicle. The cubicle surrounding the platform was controlled by a linear motor (LinMot NTI AG) with a custom-made (Electronic Workshop, University Bern) digital input/output interface, which triggered a TTL to control the cubicle moving up and down. The FAST enabled us to submit mice to sequential and separate time-locked exposures to an anxiogenic situation (an elevated, bright, and open space), a novel situation (a dark green cubicle) or a safe situation (a closed and darker cubicle).

The FAST behavioral test consists of 5 'novelty control' trials and 10 'anxiety test' trials. To avoid photon bleaching during interneurons imaging, we decided to minimize novelty controls to 5 trials to ensure that good quality of data can be obtained in the anxiety test trials. In novelty control trials, mice were first held for 20 s in the closed compartment with black background walls (safe context). Subsequently, the black cubicle was lowered, exposing mice to the green cubicle (novel context) for 30 s. During anxiety test trials, mice were held for 20 s in the closed compartment (safe). Afterwards, the black cubicle slid down to the platform base level, forcibly exposing mice to the high and brightly illuminated open compartment (anxiogenic) for 30 s. The inter trial intervals were randomized from 2 to 5 min. Head out of platform time is defined when the mouse head protrudes away from the platform edge which is assessed by a stretching neck and both ears jutting out from the platform.

Elevated plus maze (EPM). The EPM was custom-made and consisted of four arms. Each arm is 8 cm wide and 35 cm long and elevated 75 cm above the floor. The two opposing closed arms were enclosed by 18 cm high walls, whereas the other two were left open. The center zone is in the middle with a size of 8 cm × 8 cm. Prior experiments, mice were introduced into the middle part of a closed arm with head positioning

toward the center zone. Then mice explored the EPM freely for 10 min in a sound attenuating chamber under 300 lux from roof-top light. Animal positions were tracked using ANYmaze (Stoelting, USA). The mouse body center was used to define its location in closed arm, center zone or open arm of the EPM.

Open field test (OF). The open field arena consisted of four white plastic walls 40 cm high and a light gray floor (40 cm × 40 cm). The area within 10 cm from the walls is defined as the border zone and the inner 20 cm × 20 cm area is defined as the center zone. The duration of the open field test is 10 min without breaks in a sound attenuating chamber under 300 lux from roof-top light. Animals' position was tracked using ANYmaze. The mouse body center was used to define its location in the center or border zone.

Trace fear conditioning. The trace fear conditioning protocol consisted of 2 rounds of habituation (Hab) followed 4 h later by a trace fear conditioning (TFC) on day 1 in the same arena (context A) and a cued fear test (CFT) in another arena with different visual, odor and somatosensory features (context B) on day 2. Briefly, during habituation mouse freely explored context A while randomly playing 4 white noise tones (CS-, 2 s, 75 dB) and 4 pure tones (CS+, 2 s, 15 kHz, 75 dB). During trace fear conditioning, after delivering 5 CS-, foot shocks (US, 2 s, 0.6 mA) were presented through a metal grid floor 20 s (i.e., the trace) after the CS+ . The CS+ and US association was repeated 5 times to strengthen learning. On the following day, mice was tested in context B with a PVC floor while playing 4 CS- and 8 CS+ . Each habituation lasted 10 min. The trace fear conditioning protocol lasted 18 min and cued fear test lasted 22 min. Context A and context B have different lighting color and decorations on the walls. After every behavior test session, context A was cleaned with 75% ethanol and context B was cleaned with 4% acetic acid. Freezing level was calculated for 20 s after the start of CSs. ANYmaze was used to automatically detect freezing behavior and track head, tail, and body center position within the arena at 30 frames per second. The tracking engine version 7.0 and freezing detection parameters were kept consistent across all mice. Between behavioral sessions, mice remained in their home cage within a sound attenuating chamber.

Ca^{2+} imaging in freely behaving mice

Imaging sessions in freely-moving mice began 1–2 weeks after baseplating. Mice were briefly anesthetized (< 2 min) to attach the miniscope to the baseplate for each imaging day. Mice were allowed to recover from the brief anesthesia and habituate to the miniscope and behavior room for 60 min before the behavioral protocol started. Ca^{2+} imaging was performed using a miniscope (UCLA V3) or a custom-made dual-color miniscope for simultaneous Ca^{2+} imaging and optogenetic manipulation. The power of the blue laser used for GCaMP6f excitation (488 nm, Cobolt) was set to 1 mW at the tip of the miniscope objective. The power of the amber laser used for eNpHR3.0 and ChrimsonR excitation (594 nm, Cobolt) was set to 8-10 mW at the tip of the miniscope objective. The 488 nm laser was triggered by a Transistor-Transistor-Logic (TTL) signal from ANY-maze at the beginning of each recording session. The 594 nm laser was switched on according to optogenetic manipulation protocols. Ca^{2+} imaging videos were recorded at 20 Hz in uncompressed.avi format by using a data acquisition box which is triggered by an external TTL pulse from ANY-maze to synchronize Ca^{2+} imaging and behavioral tracking. The excitation power for GCaMP6f in pyramidal neurons was determined in prior tests based on the most optimal signal to noise ratio and was maintained throughout all the imaging sessions. Excitation power was sometimes slightly increased for PV interneurons imaging due to bleaching.

Optogenetic manipulation

To optogenetically manipulate ventral hippocampal neuronal activity, a laser (Cobolt) generating 594 nm amber light was attached to an optical rotary joint (Doric Lenses) to support the unrestricted movement of mice during the behavioral tests. The optical rotary joint was connected to a light splitter (Doric Lenses) to allow bilateral light delivery to two patch cables (Doric Lenses) which were in turn connected to the implanted optical fibers through a ferrule-sleeve system (Senko, USA). Light illumination was automatically controlled by ANYmaze based on the animal's body center position in the behavioral apparatus. Laser light was applied continuously at a power intensity of about 9-12 mW measured from the optical fiber tip. Before the beginning of the behavioral paradigm, mice were first connected to the patch cables for 30 min for habituation.

For the dual-color miniscope imaging, the laser source was divided into two patch cords by a light splitter, one for the optical fiber implanted into the left hemisphere, another one for dual-color miniscope into the right hemisphere. Because miniscope lost about 75% of light power through its optical pathways, the laser power for optical fiber was adjusted to similar level as at the tip of optical fiber by using an attenuating patch cord (Doric lenses). Ultimately, both brain hemispheres received approximately 9–12 mW laser light power.

For FAST, the optogenetic laser light was switched on for 30 s when the black cubicle was dropped down at certain trials, namely the 9^{th}, 10^{th}, 11^{th}, 15^{th}, 16^{th}, 17^{th} trials. For EPM, the optogenetic laser light was switched on whenever the mice body center was in the center zone or open arm during 121–240 s, 361–480 s, 601–720 s in a 14-minutes long protocol. During trace fear conditioning, laser light was switched on 1 s before CS+ and lasted 27 s, covering the whole CS+ , trace interval and US periods for pyramidal neurons, VIP and Sst interneurons stimulation. For PV interneurons inhibition, optogenetic laser light was switched on 1 s before the US and lasted 5 s.

Immunohistochemistry

Mice were overdosed with a ketamine/xylazine cocktail and transcardially perfused with phosphate-buffered saline (PBS) followed by 4% formaldehyde. The brains were removed and fixed in 4% PFA for 24 h at 4 °C. Brains were sectioned coronally at a thickness of 50 µm using a vibratome (Leica Microsystems, VT1000 S). The immunostaining was performed on free-floating brain slices. The sections were incubated in a blocking buffer containing 5% normal donkey serum (Jackson Immuno Research, Dianova) and 0.1% Triton-X 100 (Sigma, USA) in PBS for 1 h to prevent nonspecific background staining. After blocking, the sections were incubated with the primary antibodies diluted in the blocking buffer. The following primary antibodies were used: anti-GFP polyclonal antibodies (Rockland 600-101-215, 1:2000; Invitrogen A11122, 1:2000), anti-Parvalbumin monoclonal antibody (Synaptic Systems, 195308, 1:1000), anti-Somatostatin monoclonal antibody (Invitrogen MA516987, 1:500; Millipore MAB354, 1:500), anti-VIP polyclonal antibody (Invitrogen PA578224, 1:500), anti-RFP monoclonal antibody (Invitrogen MA515257, 1:1000). After overnight incubation with primary antibodies at 4 °C, the sections were rinsed in PBS three times for 10 min each and incubated with secondary antibodies (2% BSA and 1% Triton-X 100 in PBS) for 2 h in the dark at room temperature. The secondary antibodies were as follows: Goat anti-Rabbit IgG-conjugated Alexa Fluor 633 (A21070), Goat anti-Guinea Pig IgG-conjugated Alexa Fluor 633 (A21105), Donkey anti-Rabbit IgG-conjugated Alexa Fluor 405 (A48258), Donkey anti-Rat IgG-conjugated Alexa Fluor 405 (A48268), Donkey anti-Rat IgG-conjugated Alexa Fluor 594 (A21209), Donkey anti-Rabbit IgG-conjugated Alexa Fluor 594 (A21207), Donkey anti-Rabbit IgG-conjugated Alexa Fluor 488 (A21206), Goat anti-Guinea Pig IgG-conjugated Alexa Fluor 594 (A11076), all purchased from Invitrogen used in dilution of 1:1000. Afterwards, the sections were washed three times in PBS for 10 min, transferred to Superfrost Plus charged glass slides, and mounted in Vectashield mounting medium (Vector Laboratories, USA).

Microscopy and cell quantification

Immunolabelled sections were imaged using LSM 880 Airyscan confocal laser scanning microscope (Zeiss, Germany). For rabies tracing experiments, all brain sections between bregma −3.08 mm and −3.52 mm were immunolabelled for VIP, PV or Sst antibodies with different combinations. The GFP and tdTomato positive cells corresponded to starter cells. tdTomato only positive cells were presynaptic cells targeting PV or Sst interneurons. The multichannel image stacks were processed manually in ImageJ. 3D stacks were split into each channel of GFP, tdTomato, VIP-Alexa 405, PV-Alexa 633, Sst-Alexa 633. Then all channel images were synchronized in ImageJ and analyzed colocalization based on cell morphology and intensity level compared to surrounding neuropil. All GFP positive neurons were excluded from analysis. The percentage of presynaptic input neurons was calculated as: (number of VIP/PV/Sst positive and tdTomato positive neurons/ total tdTomato positive neurons) × 100.

Ca^{2+} imaging data extraction

Only mice with verified viral expression and GRIN lens placements in the target sites were included in the analyses. Ca^{2+} imaging videos were analyzed using a custom-made Matlab code[25]. Videos from multiple sessions were concatenated and downsampled by a binning factor of 4 resulting in a frame rate of 5 Hz, and lateral brain movements were motion-corrected using the Turboreg algorithm (Thévenaz et al., 1998). Fluorescent traces were extracted by applying automatically detected individual cell filters based on combined principal and individual component analysis (PCA/ICA) as described in (Mukamel et al., 2009). This approach combines spatial and temporal statistics and precedes ICA and PCA, to reduce data dimensionality and to support ICA in finding global optima. The overall procedure is proved to be effective from grounded hypotheses: cellular signals are mathematically separable into products of paired spatial and temporal components; signals from different cells are statistically independent; and cells' spatial filters and temporal signals have skewed distributions. In brief, this automated sorting procedure combines ICA and image segmentation for extracting cells' locations and their dynamics with minimal human supervision. To control for non-inclusion of split neurons in our analyses, we identified pairs of neurons with highly correlated activity (Pearson correlation > 0.7) that were spatially close (centroid distance < 20 pixels) and excluded one of the neurons for each pair. Identified putative neurons were then sorted via visual inspection to select neurons with appropriate somatic morphology and Ca^{2+} dynamics.

Neuronal activity analysis

Relative changes in Ca^{2+} fluorescence (F) were calculated using the formula: $\Delta F/F_0 = (F-F_0) / F_0$ (F_0 = the fluorescence intensity over the entire trace) and used for all the analyses of Ca^{2+} activity. Ca^{2+} transient level was used as a proxy of neuronal activity. The neuronal activity level was presented as integral of area under the curve of Ca^{2+} transient normalized by the time of the corresponding period (AUC/s). Ca^{2+} signal that was 3 times higher than the standard deviation (SD) of the entire trace was considered as a relevant neuronal activity. All analyses were done on z-scored traces.

Anxiety neurons. To identify neurons' responsiveness to the anxiogenic context on FAST, the neuronal activity in the anxiogenic context (open compartment) or a novel context (dark green cubicle) was first subtracted to the activity in safe context (black cubicle) corresponding to a baseline spontaneous activity. Then the activity in the anxiogenic context was compared to the activity in the novel context. As the FAST is a trial-based anxiety task, we developed a 2-step criterion to evaluate the responsiveness of neurons to anxiety-eliciting conditions. First, within each trial, an anxiety neuron should exhibit a significantly higher activity level than the background activity, i.e., calcium signals are 3 times SD larger than the normalized mean of the entire Ca^{2+} trace. Second, we introduced another criterion relating to the 'response probability' due to the trial-based nature of FAST to avoid the detection of false positive neurons caused by a very large response in one single trial which would bring up the averaged activity across all trials. An anxiety neuron should faithfully respond to the anxiogenic context with at least 40% (e.g., 4 in 10 test trials) but less than 40% to the novel context (e.g., 2 in 5 control trials). Note that as the FAST has a limited area of exploration for mice, we normalized the total neuronal activity to 30 s, corresponding to the entire time of exposure to the anxiogenic context.

On the EPM, the neuronal activity was calculated by normalizing the integral of Ca^{2+} transients in closed, center or open arms to the corresponding exploration time. Then the normalized activity in the center or open arms was compared to the activity in the closed arm. Mice freely explored the EPM compartments and Ca^{2+} activity can be registered at anytime and anywhere during the entire EPM exploration. Therefore, we normalized the total Ca^{2+} activity of each EPM compartment exploration to the corresponding time of exploration, allowing to compare normalized Ca^{2+} activity per time unit across the close, center and open compartments of the EPM. Neurons showing higher activity in the open arms, but not activated in closed arms were considered to be anxiety neurons. The same criteria was used for OF by comparing neuronal activity in the center and border zones.

Fear neurons. To identify fear neurons, we compared neuronal activity to the CS+ with the activity to the CS- during cued fear test in context B. For CS+ activated fear neurons, we also applied a 2-step criterion by firstly identifying whether neurons significantly respond to the cue and then quantify the response probability. In practice, fear neurons should show a significantly higher activity than baseline activity (3 SD higher than the averaged Ca^{2+} activity of the entire trace) and responded to the CS+ more than 25% of the trials (more than 2 trials out of the total of 8 CS+ trials), but not more than 25% of the trials to the CS- (maximally 1 in the total of 4 CS- trials). The activity to the CS-, CS+ and US was considered for 2 s, starting from the onset of the stimuli.

For multi-session analyses, Ca^{2+} imaging videos from the FAST and cued fear test (CFT) sessions or Ca^{2+} imaging videos from EPM, FAST and OF were concatenated and traces were extracted for the same individual neurons[25,70]. Then, the Ca^{2+} traces for individual neurons were split into traces for individual behavioral tasks according to the recording timestamps. The activity of each neuron was analyzed individually for anxiety and fear responsive neurons according to the criteria described above. Finally, individual neurons were classified as anxiety neurons, fear neurons, anxiety and fear overlapping neurons, or non-responding neurons based on significant task activity.

Statistics and Reproducibility

Analyses were performed using custom scripts written in MATLAB (MathWorks). Statistics were performed using GraphPad Prism 9. All datasets were tested for normality using the Kolmogorov-Smirnov test or Shapiro-Wilk test based on sample size. Normally distributed data undergo parametric tests, otherwise nonparametric tests were applied. All null hypothesis tests were two-sided. Analyses of variance (ANOVAs) were followed by post hoc tests if a main effect or interaction was observed. Box and whisker plots show median and interquartile range (minima, 25th and 75th percentile, and maxima). Bar graphs show data as means ± SEM. Asterisks in the figures represent P values corresponding to the following thresholds: $^{*}P < 0.05$; $^{**}P < 0.01$; $^{***}P < 0.001$. All statistics are listed in Supplementary Table 1.

Representative experiments for instance in Figs. 3a, c and 4a, s were repeated over many sections using confocal microscopy in 4 to 10 mice.

Reporting summary

Further information on research design is available in the Nature Portfolio Reporting Summary linked to this article.

Data availability

Source data are provided with this paper. The original data used in this study are available in Figshare repository under open access licence CC BY 4.0. https://doi.org/10.6084/m9.figshare.26575084. Additional data relating to this paper are available upon request, because of the size (6.5 TB) of the calcium imaging and animal behavioral tracking data is too large to be deposited online. Source data are provided with this paper.

Code availability

The Matlab code used for Ca^{2+} signal extraction is available from B. Grewe lab[25]. The Matlab code for AUC analysis used in this study is deposited in Figshare, https://doi.org/10.6084/m9.figshare.26575084.

References

1. LeDoux, J. E. Emotion Circuits in the Brain. *Annu. Rev. Neurosci.* **23**, 155–184 (2000).
2. Mobbs, D., Headley, D. B., Ding, W. & Dayan, P. Space, time, and fear: survival computations along defensive circuits. *Trends Cogn. Sci.* **24**, 228–241 (2020).
3. Anderson, D. J. & Adolphs, R. A framework for studying emotions across species. *Cell* **157**, 187–200 (2014).
4. Malezieux, M., Klein, A. S. & Gogolla, N. Neural circuits for emotion. *Annu Rev. Neurosci.* **46**, 211–231 (2023).
5. Maren, S., Phan, K. L. & Liberzon, I. The contextual brain: implications for fear conditioning, extinction and psychopathology. *Nat. Rev. Neurosci.* **14**, 417–428 (2013).
6. Calhoon, G. G. & Tye, K. M. Resolving the neural circuits of anxiety. *Nat. Neurosci.* **18**, 1394–1404 (2015).
7. Tovote, P., Fadok, J. P. & Luthi, A. Neuronal circuits for fear and anxiety. *Nat. Rev. Neurosci.* **16**, 317–331 (2015).
8. Adhikari, A., Topiwala, M. A. & Gordon, J. A. Single units in the medial prefrontal cortex with anxiety-related firing patterns are preferentially influenced by ventral hippocampal activity. *Neuron* **71**, 898–910 (2011).
9. Botta, P. et al. Regulating anxiety with extrasynaptic inhibition. *Nat. Neurosci.* **18**, 1493–1500 (2015).
10. Felix-Ortiz, A. C. et al. BLA to vHPC inputs modulate anxiety-related behaviors. *Neuron* **79**, 658–664 (2013).
11. Felix-Ortiz, A. C., Burgos-Robles, A., Bhagat, N. D., Leppla, C. A. & Tye, K. M. Bidirectional modulation of anxiety-related and social behaviors by amygdala projections to the medial prefrontal cortex. *Neuroscience* **321**, 197–209 (2016).
12. Forro, T. et al. Anxiety-related activity of ventral hippocampal interneurons. *Prog. Neurobiol.* **219**, 102368 (2022).
13. Kim, W. B. & Cho, J. H. Encoding of contextual fear memory in hippocampal-amygdala circuit. *Nat. Commun.* **11**, 1382 (2020).
14. Kjelstrup, K. G. et al. Reduced fear expression after lesions of the ventral hippocampus. *Proc. Natl Acad. Sci.* **99**, 10825–10830 (2002).
15. Mikulovic, S. et al. Ventral hippocampal OLM cells control type 2 theta oscillations and response to predator odor. *Nat. Commun.* **9**, 3638 (2018).
16. Sotres-Bayon, F., Sierra-Mercado, D., Pardilla-Delgado, E. & Quirk, G. J. Gating of fear in prelimbic cortex by hippocampal and amygdala inputs. *Neuron* **76**, 804–812 (2012).
17. Tye, K. M. et al. Amygdala circuitry mediating reversible and bidirectional control of anxiety. *Nature* **471**, 358–362 (2011).
18. Ciocchi, S., Passecker, J., Malagon-Vina, H., Mikus, N. & Klausberger, T. Selective information routing by ventral hippocampal CA1 projection neurons. *Science* **348**, 560–563 (2015).
19. Jimenez, J. C. et al. Anxiety cells in a hippocampal-hypothalamic circuit. *Neuron* **97**, 670–683.e676 (2018).
20. Padilla-Coreano, N. et al. Direct ventral hippocampal-prefrontal input is required for anxiety-related neural activity and behavior. *Neuron* **89**, 857–866 (2016).
21. Xu, C. et al. Distinct hippocampal pathways mediate dissociable roles of context in memory retrieval. *Cell* **167**, 961–972.e916 (2016).
22. Jimenez, J. C. et al. Contextual fear memory retrieval by correlated ensembles of ventral CA1 neurons. *Nat. Commun.* **11**, 3492 (2020).
23. Löw, K. et al. Molecular and neuronal substrate for the selective attenuation of anxiety. *Science* **290**, 131–134 (2000).
24. Cai, D. J. et al. A shared neural ensemble links distinct contextual memories encoded close in time. *Nature* **534**, 115–118 (2016).
25. Grewe, B. F. et al. Neural ensemble dynamics underlying a long-term associative memory. *Nature* **543**, 670–675 (2017).
26. Koukoutselos, K. Anticipatory coding of anxiety in the ventral hippocampus. Universität Bern, Grad-verleihende Institution Bern. Schweizerische Nationalbibliothek, Magazin Ost; Nbq 140821 (2023).
27. Huerta, P. T., Sun, L. D., Wilson, M. A. & Tonegawa, S. Formation of temporal memory requires NMDA receptors within CA1 pyramidal neurons. *Neuron* **25**, 473–480 (2000).
28. Herbst, M. R., Twining, R. C. & Gilmartin, M. R. Ventral hippocampal shock encoding modulates the expression of trace cued fear. *Neurobiol. Learn Mem.* **190**, 107610 (2022).
29. Klausberger, T. & Somogyi, P. Neuronal diversity and temporal dynamics: the unity of hippocampal circuit operations. *Science* **321**, 53–57 (2008).
30. Letzkus, J. J., Wolff, S. B. & Luthi, A. Disinhibition, a circuit mechanism for associative learning and memory. *Neuron* **88**, 264–276 (2015).
31. Pelkey, K. A. et al. Hippocampal GABAergic Inhibitory Interneurons. *Physiol. Rev.* **97**, 1619–1747 (2017).
32. Singh, S. & Topolnik, L. Inhibitory circuits in fear memory and fear-related disorders. *Front Neural Circuits* **17**, 1122314 (2023).
33. Leao, R. N. et al. OLM interneurons differentially modulate CA3 and entorhinal inputs to hippocampal CA1 neurons. *Nat. Neurosci.* **15**, 1524–1530 (2012).
34. Srinivasan, S. et al. Miniaturized microscope with flexible light source input for neuronal imaging and manipulation in freely behaving animals. *Biochem Biophys. Res Commun.* **517**, 520–524 (2019).
35. Bezaire, M. J. & Soltesz, I. Quantitative assessment of CA1 local circuits: knowledge base for interneuron-pyramidal cell connectivity. *Hippocampus* **23**, 751–785 (2013).
36. Booker, S. A. & Vida, I. Morphological diversity and connectivity of hippocampal interneurons. *Cell Tissue Res* **373**, 619–641 (2018).
37. Rudy, B., Fishell, G., Lee, S. & Hjerling-Leffler, J. Three groups of interneurons account for nearly 100% of neocortical GABAergic neurons. *Dev. Neurobiol.* **71**, 45–61 (2011).
38. Pi, H. J. et al. Cortical interneurons that specialize in disinhibitory control. *Nature* **503**, 521–524 (2013).
39. Krabbe, S. et al. Adaptive disinhibitory gating by VIP interneurons permits associative learning. *Nat. Neurosci.* **22**, 1834–1843 (2019).
40. Hu, H., Gan, J. & Jonas, P. Fast-spiking, parvalbumin+ GABAergic interneurons: from cellular design to microcircuit function. *Science* **345**, 1255263 (2014).
41. Deng, X., Gu, L., Sui, N., Guo, J. & Liang, J. Parvalbumin interneuron in the ventral hippocampus functions as a discriminator in social memory. *Proc. Natl Acad. Sci. USA* **116**, 16583–16592 (2019).
42. Volitaki, E. et al. Activity of ventral hippocampal parvalbumin interneurons during anxiety. *Cell Rep.* **43**, 114295 (2024).
43. Klausberger, T., Roberts, J. D. B. & Somogyi, P. Cell Type- and input-specific differences in the number and subtypes of synaptic $GABA_A$ receptors in the hippocampus. *J. Neurosci.* **22**, 2513–2521 (2002).

44. Roy, D. S. et al. Distinct neural circuits for the formation and retrieval of episodic memories. *Cell* **170**, 1000–1012 e1019 (2017).
45. Tanaka, K. Z. et al. The hippocampal engram maps experience but not place. *Science* **361**, 392–397 (2018).
46. Josselyn, S. A. & Tonegawa, S. Memory engrams: recalling the past and imagining the future. *Science* **367**, eaaw4325 (2020).
47. Lovett-Barron, M. et al. Dendritic inhibition in the hippocampus supports fear learning. *Science* **343**, 857–863 (2014).
48. Bilash, O. M., Chavlis, S., Johnson, C. D., Poirazi, P. & Basu, J. Lateral entorhinal cortex inputs modulate hippocampal dendritic excitability by recruiting a local disinhibitory microcircuit. *Cell Rep.* **42**, 111962 (2023).
49. Szonyi, A. et al. Brainstem nucleus incertus controls contextual memory formation. *Science* **364**, eaaw0445 (2019).
50. Topolnik, L. & Tamboli, S. The role of inhibitory circuits in hippocampal memory processing. *Nat. Rev. Neurosci.* **23**, 476–492 (2022).
51. Dannenberg, H. et al. Synergy of direct and indirect cholinergic septo-hippocampal pathways coordinates firing in hippocampal networks. *J. Neurosci.* **35**, 8394–8410 (2015).
52. Teles-Grilo Ruivo, L. M. & Mellor, J. R. Cholinergic modulation of hippocampal network function. *Front Synaptic Neurosci.* **5**, 2 (2013).
53. Yoshida, K., Drew, M. R., Mimura, M. & Tanaka, K. F. Serotonin-mediated inhibition of ventral hippocampus is required for sustained goal-directed behavior. *Nat. Neurosci.* **22**, 770–777 (2019).
54. Honore, E., Khlaifia, A., Bosson, A. & Lacaille, J. C. Hippocampal somatostatin interneurons, long-term synaptic plasticity and memory. *Front Neural Circuits* **15**, 687558 (2021).
55. Muller, C. & Remy, S. Dendritic inhibition mediated by O-LM and bistratified interneurons in the hippocampus. *Front Synaptic Neurosci.* **6**, 23 (2014).
56. Katona, L. et al. Sleep and movement differentiates actions of two types of somatostatin-expressing GABAergic interneuron in rat hippocampus. *Neuron* **82**, 872–886 (2014).
57. Tyan, L. et al. Dendritic inhibition provided by interneuron-specific cells controls the firing rate and timing of the hippocampal feedback inhibitory circuitry. *J. Neurosci.* **34**, 4534–4547 (2014).
58. Basu, J. & Siegelbaum, S. A. The corticohippocampal circuit, synaptic plasticity, and memory. *Cold Spring Harb Perspect Biol.* **7**, a021733 (2015).
59. Turi, G. F. et al. Vasoactive intestinal polypeptide-expressing interneurons in the hippocampus support goal-oriented spatial learning. *Neuron* **101**, 1150–1165.e1158 (2019).
60. Kitamura, T. et al. Island cells control temporal association memory. *Science* **343**, 896–901 (2014).
61. Nguyen, R., Koukoutselos, K., Forro, T. & Ciocchi, S. Fear extinction relies on ventral hippocampal safety codes shaped by the amygdala. *Sci. Adv.* **9**, eadg4881 (2023).
62. Adhikari, A., Topiwala, M. A. & Gordon, J. A. Synchronized activity between the ventral hippocampus and the medial prefrontal cortex during anxiety. *Neuron* **65**, 257–269 (2010).
63. Sanchez-Bellot, C., AlSubaie, R., Mishchanchuk, K., Wee, R. W. S. & MacAskill, A. F. Two opposing hippocampus to prefrontal cortex pathways for the control of approach and avoidance behaviour. *Nat. Commun.* **13**, 339 (2022).
64. Parfitt, G. M. et al. Bidirectional Control of anxiety-related behaviors in mice: role of inputs arising from the ventral hippocampus to the lateral septum and medial prefrontal cortex. *Neuropsychopharmacology* **42**, 1715–1728 (2017).
65. Jackson, A. D. et al. Amygdala-hippocampus somatostatin interneuron beta-synchrony underlies a cross-species biomarker of emotional state. *Neuron* **112**, 1182–1195.e1185 (2024).
66. Lee, S. H. et al. Parvalbumin-positive basket cells differentiate among hippocampal pyramidal cells. *Neuron* **82**, 1129–1144 (2014).
67. Marin, O. Interneuron dysfunction in psychiatric disorders. *Nat. Rev. Neurosci.* **13**, 107–120 (2012).
68. Aime, M. et al. Paradoxical somatodendritic decoupling supports cortical plasticity during REM sleep. *Science* **376**, 724–730 (2022).
69. d'Aquin, S. et al. Compartmentalized dendritic plasticity during associative learning. *Science* **376**, eabf7052 (2022).
70. Gründemann, J. et al. Amygdala ensembles encode behavioral states. *Science* **364**, eaav8736 (2019).

Acknowledgements

We thank Benjamin Grewe (ETHZ, Switzerland) for providing the Ca^{2+} signal extraction toolset; Christian Dellenbach for electronic assistance and Michael Känzig for animal breeding; Thomas Forro (University of Bern, Switzerland) and Johannes Letzkus (University of Freiburg, Germany) for discussions. This study was supported by a European Research Council starting grant 716761 (SC), Swiss National Science Foundation professorship grant 170654 (SC), Swiss National Science Foundation Flexibility Grant (KL), Novartis Foundation for medical-biological Research 24A021 (KL), and Japan Agency for Medical Research and Development JP23zf0127005, JP23km0908001 (MS).

Author contributions

Conceptualization: K.L., S.C.; Methodology: K.L., M.S., K.K. (FAST); Investigation: K.L.; Visualization: K.L.; Funding acquisition: S.C.; Project administration: K.L.; Supervision: S.C.; Writing–original draft: K.L., S.C.; Writing–review & editing: K.L., S.C., K.K., M.S.

Competing interests

The authors declare no competing interests.

Additional information

Supplementary information The online version contains supplementary material available at https://doi.org/10.1038/s41467-024-52466-4.

Correspondence and requests for materials should be addressed to Kaizhen Li or Stéphane Ciocchi.

Peer review information *Nature Communications* thanks Nadine Gogolla and the other, anonymous, reviewer for their contribution to the peer review of this work. A peer review file is available.